Arabian Journal of Chemistry (2022) **15**, 103549

King Saud University

Arabian Journal of Chemistry

www.ksu.edu.sa
www.sciencedirect.com

ORIGINAL ARTICLE

One-step fabrication of hydrophilic lignosulfonate-decorated reduced graphene oxide to enhance the pervaporation performance of calcium alginate membranes

Saisai Li [a], Yaru Wu [a], Xia Zhan [b], Jiding Li [c], Jiandu Lei [a], Jing He [d,*], Luying Wang [a,*]

[a] *Beijing Key Laboratory of Lignocellulosic Chemistry, Beijing Forestry University, Beijing 100083, China*
[b] *Key Laboratory of Cleaner Production and Integrated Resource Utilization of China National Light Industry, Beijing Technology and Business University, Beijing 100048, China*
[c] *Department of Chemical Engineering, Tsinghua University, Beijing 100084, China*
[d] *MOE Engineering Research Center of Forestry Biomass Materials and Bioenergy, Beijing Forestry University, Beijing 100083, China*

Received 13 September 2021; accepted 7 November 2021
Available online 12 November 2021

KEYWORDS

Reduced graphene oxide;
Calcium alginate;
Pervaporation;
Membranes;
Alcohol

Abstract In this study, a reduced graphene oxide (rGO)@sodium lignosulfonate (NaLS) composite material was fabtricated using a one-step method and then mixed with natural polysaccharide calcium alginate (CaAlg) to prepare the rGO@NaLS/CaAlg pervaporation membrane. The appearance and physical properties of the rGO@NaLS/CaAlg membrane were characterized by scanning electron microscopy and water contact angle. The swelling performance of the membrane and its dehydration performance to organic solvents were evaluated. The results indicate that the addition of rGO@NaLS can increase the hydrophilicity of the rGO@NaLS/CaAlg membrane and reduce its degree of swelling in the ethanol solution. The membrane incorporated with 6 wt% rGO@NaLS exhibits the best pervaporation performance, and ethanol can be purified to 99.8%.

1. Introduction

Graphene is a new material in which carbon atoms connected by sp (Zhao et al., 2021) hybridization are closely packed into a single-layer two-dimensional honeycomb lattice structure (Liu et al., 2019). Graphene exhibits excellent characteristics such as low density and high specific surface area, and exhibits potential for application in materials science (Zhao et al., 2021;

* Corresponding authors.
E-mail address: wangly@bjfu.edu.cn (L. Wang).
Peer review under responsibility of King Saud University.

Production and hosting by Elsevier

https://doi.org/10.1016/j.arabjc.2021.103549
1878-5352

Mirabedini et al., 2020; Zhao et al., 2019; Tong et al., 2020; Yu et al., 2020), energy (Liu et al., 2019; Chen et al., 2021), and biomedicine (Shende and Pathan, 2020; Ma et al., 2019). Graphene is a perfect network composed of infinitely conjugated carbon–carbon double bonds (Fig. 1**a**), which is the reason for the excellent performance of graphene materials. Graphene oxide (GO) is dotted with a large number of oxygen-containing groups on this network, which destroys the conjugated structure of graphene and causes pore damage **(**Fig. 1**b)**. That by the reduction process of graphene oxide it can be eliminated its oxygen-containing groups and thus form a rGO. (Eigler and Hirsch, 2014) (Fig. 1**c**)

Li et al (Qiu et al., 2011). used vacuum filtration to prepare a reduced graphene membrane for liquid phase separation, and the water flux reached 4 $m^{-2}{\cdot}h^{-1}{\cdot}bar^{-1}$, indicating good selectivity for nano-gold and nano-platinum particles. The carbon-rich regions between adjacent rGO layers can form hydrophobic channels similar to carbon nanotubes (Sheng et al., 2020), and there are pores on the surface of each layer, which is a superior water-permeable material. Based on the structural characteristics of rGO, it can also be used as an excellent material to improve performance of dehydration membrane. (Hamzah et al., 2020; Fan et al., 2019; Zhang et al., 2018; Safarpour et al., 2015) However, the distance between rGO sheets is short, has strong Van der Waals force, easy to agglomerate, and exhibits poor dispersion in water (Guo et al., 2013), considerably limiting the application of rGO. Improving the dispersion of rGO and widening the spacing of rGO layers are problems that need to be solved present.

Lignin is a general term for a large number of aromatic polymers produced by the oxidative combinatorial coupling of 4-hydroxyphenylpropanoids and is one of most abundant biopolymers on the planet (Kai et al., 2017). Lignosulfonate is a lignin derivative derived from papermaking waste, it has a three-dimensional molecular structure and amphiphilic properties, and is highly sensitive to water molecules (Li et al., 2016; Liu et al., 2015). There have been studies using lignosulfonate as a modified filler to improve membrane performance (Li et al., 2021; Guan et al., 2018). This study mainly uses lignosulfonate as a surfactant to modify rGO. As shown in Fig. 2, the rGO@NaLS composite material can be prepared simply and quickly by a one-step method. Lignosulfonate is compounded with rGO sheets to destroy the van der Waals force between the rGO sheets, expand its pores, and increase the hydrophilicity of the rGO material (Chen et al., 2018), making full use of the pores on the rGO layer, combining the advantage of both, can be used as an efficient water-permeable filler for pervaporation membrane.

Alginate is a natural polysaccharide extracted from brown algae, which exhibits good biodegradability and hydrophilicity. Kuzminova et al (Kuzminova et al., 2021). developed a dense and supported (polyacrylonitrile substrate) mixed matrix membrane based on sodium alginate, modified with UiO-66 to improve the pervaporation dehydration performance of the isopropanol. The transmission characteristics of dense and supporting membranes were tested, and the permeation flux reached 0.47–3.38 $kg{\cdot}m^{-2}{\cdot}h^{-1}$, and the water content in the permeate was 99.9–97.5 wt%. However, pure alginate has an uneven structure and poor strength (Li et al., 2019), and its separation performance requires further improvement. One of the effective ways to enhance its performance is by introducing nanomaterials into alginate (Kuzminova et al., 2021; Liu et al., 2019; Park et al., 2019; Cao et al., 2019). The previous also tried to use nano-sheet materials to improve the performance of the CaAlg membrane, and the pervaporation performance was significantly improved (Li et al., 2021). However, the surface of the MXene sheet material is dense and there are no pores (Ding et al., 2018), so rGO@NaLS composite material has the potential to further improve the CaAlg membrane.

In the current study, an rGO@NaLS composite material was prepared by chemical reduction and incorporation into sodium alginate (NaAlg). By calcium alginate cross-linking, a NaAlg-based rGO@NaLS/CaAlg membrane was fabricated. The addition of rGO@NaLS composite material improved the flexibility and water permeability of pure CaAlg membrane, allowing molecules to quickly diffuse into the three-dimensional space of the membrane. These characteristic providers the ability to overcome the "trade-off" effect during membrane separation, thereby obtaining a superior pervaporation membrane.

2. Experimental

2.1. Materials

NaAlg was supplied by Aladdin Industrial Corporation. (Shanghai, China). NaLS was purchased from Sigma-Aldrich Chemicals Co, Ltd. (USA). GO suspension was received from

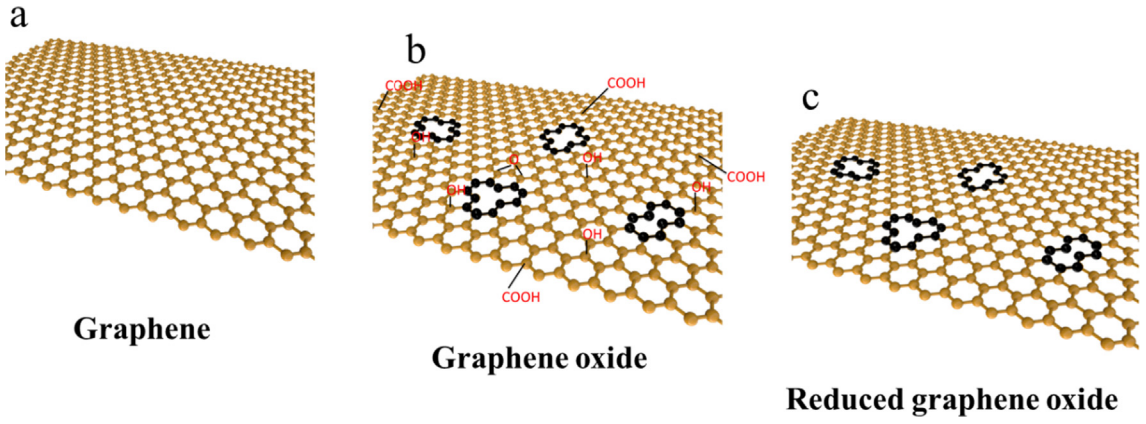

Fig. 1 Schematic diagram of graphene structure material.

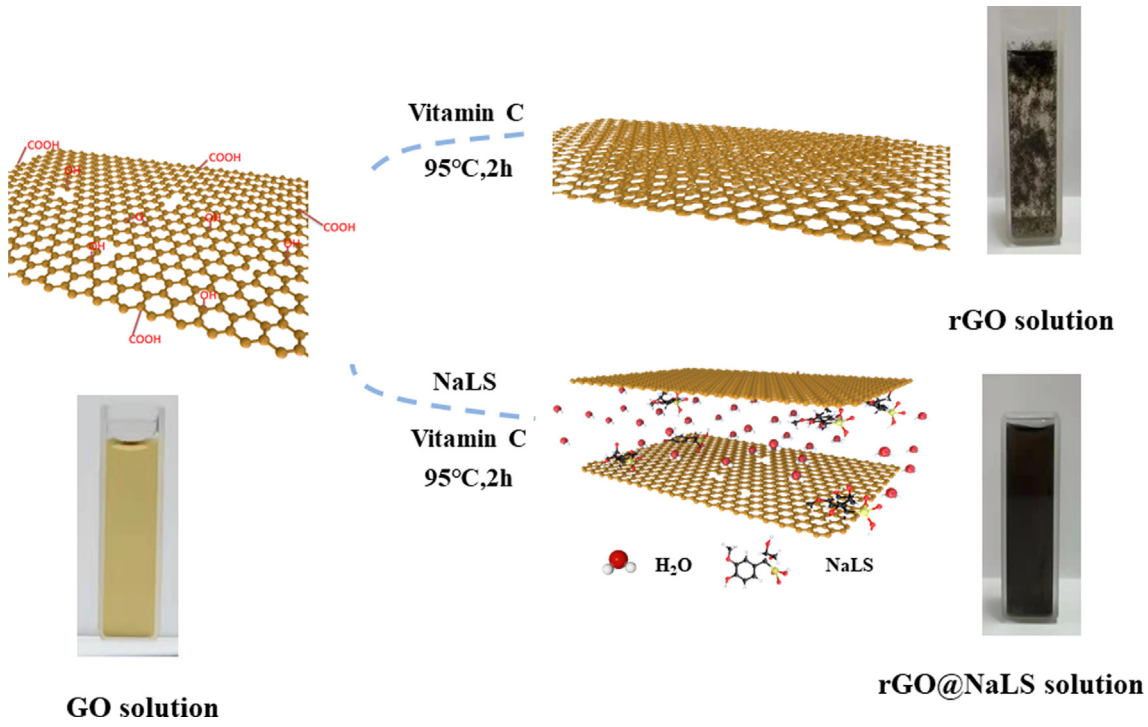

Fig. 2 Comparison chart showing the preparation of GO. rGO, and rGO@NaLS composite material.

Hengqiu Technology Industrial Corporation. (Suzhou, China). Ethanol (>99.7%) was supplied by Modern Oriental (Beijing) Technology Development Co, Ltd. (Beijing, China). Calcium chloride ($CaCl_2{\cdot}2H_2O$) was supplied by Aladdin Industrial Corporation. (Shanghai, China). Vitamin C was offered by Coolaber Science & Technology Co, Ltd. (Beijing, China). Polyacrylonitrile (PAN) ultrafiltration membrane was obtained from Shanghai Lanjing Membrane Technology Engineering Co, Ltd. (Shanghai, China).

2.2. Preparation of rGO@NaLS composite material

Dissolve GO nanosheets and NaLS in deionized water (40 ml) at a certain mass ratio (1/16), and sonicate for a period of time to make them uniformly mixed. Add vitamin C (0.1 $mg{\cdot}ml^{-1}$) to the above mixture, and reacted at 95 ℃ for 2 h (vigorous stirring). Cool the reacted mixed solution to room temperature and sonicate for 1 h to obtain a black homogeneous solution, namely rGO@NaLS mixed solution, which can be further obtained by vacuum filtration to obtain rGO@NaLS power. (Chen et al., 2018).

2.3. Preparation of rGO@NaLS/CaAlg membranes

Approximately 1 wt% NaAlg powder was dissolved in the rGO@NaLS composite material, magnetically stirred until uniformity was reached, and allowed to stand for 24 h to eliminate bubbles. The obtained rGO@NaLS/NaAlg membrane solution was cast on the PAN ultrafiltration membrane to form a membrane, and then placed in a 0.5 M $CaCl_2$ aqueous solution for cross-linking for 1 h. The cross-linked membrane was then rinsed repeatedly with deionized water, and the excess water on the membrane surface was removed with filter paper to obtain the rGO@NaLS/CaAlg membrane. The rGO@NaLS contents were 0, 2, 6, 8 and 10 wt%.

2.4. Swelling experiments

The stability of the membrane in the ethanol solvent was evaluated. CaAlg, rGO/CaAlg and rGO@NaLS/CaAlg dense membrane were prepared (the dense membrane was prepared by casting directly on the glass plate). After being dried at room temperature, the membrane was placed in an oven to dry for 72 h (100℃) and then weighed. The membrane was immersed in 80 wt%, 85 wt%, 90 wt% and 95 wt% ethanol solutions, respectively, and then allowed to stand for 72 h. The excess solvent was quickly removed from the surface and then weighed. To reduce the error, the experiment was repeated several times. The swelling degree S (wt%) is expressed by the following formula:

$$S = \frac{W_S - W_D}{W_D} \times 100\% \quad (1)$$

where W_S (g) and W_D (g) are the weights of the rGO@NaLS/CaAlg membrane after and before swelling experiments.

For a scientific analysis membrane pervaporation process, the CaAlg, rGO/CaAlg and rGO@NaLS/CaAlg membranes were placed in deionized water to measure the swelling. The process and calculation formula are consistent with the above aforementioned swelling experiment.

2.5. Characterizations

The crystal structure and molecular structure of the rGO@NaLS composite material were characterized by X-ray diffraction (XRD, Ultima IV, Japan) and Fourier transform infrared

spectroscopy (FTIR, Nicolet iS 10, Germany). Atomic force microscopy (AFM, Brook, Multimode 8, Brook, USA) was used to observe the flake structure of the rGO@NaLS composite material. The morphology of the rGO@NaLS/CaAlg membrane was characterized by scanning electron microscopy (SEM, JSM-7610, Japan). The water contact angle of the membrane was measured with a contact angle measuring instrument (CA, LAUDA Scientific, Germany).

2.6. Pervaporation experiments

The rGO@NaLS/CaAlg membrane was placed in the permeation cell, and the temperature of the digital display was set to 40-70℃. The feed liquid was 90 wt% ethanol solution, the feed flow rate was 2 L/min, and the cycle was repeated from the feed liquid pump via the membrane side. The pervaporation device used a plane cross-flow, the effective membrane area was about 0.0023 m^2, and the permeated vapor was collected by a liquid nitrogen cold trap. To reduce errors, each test was collected at least 3 times. Gas chromatography was performed to analyze the ethanol concentration, and the weight of the permeation was determined using an electronic analytical balance. The performance analysis of the membrane usually adopts the following formulae

$$J = \frac{Q}{At} \tag{2}$$

where J represents the permeation flux, Q (g) is the total mass of the permeate collected during time t (h), and A (m^2) denotes the effective area of the membrane.

$$\alpha = \frac{Y_A X_B}{X_A Y_B} \tag{3}$$

where α represents the separation factor, X_A and X_B denote the ethanol and water concentrations (wt%) in the feed solution respectively, and Y_A and Y_B are the ethanol and water concentrations (wt%) in the permeate.

3. Results and discussion

3.1. Characterization of the rGO@NaLS composite material

3.1.1. rGO composite material dispersibility

As shown in Fig. 2, rGO and rGO@NaLS composite materials are prepared by reducing graphene oxide (GO). Compared with GO, rGO substantially reduces hydrophilic groups, exhibits poor dispersion, and is agglomerated and suspended in water. After NaLS is added during the reduction, by the combination of NaLS and rGO, the hydrophilic group of rGO@NaLS increases, and the dispersibility is considerably improved. The composite material shows excellent water dispersion, and can be used fully mixed with the CaAlg matrix.

3.1.2. X-ray diffraction and Fourier transform infrared spectroscopy

The crystal structure of the rGO@NaLS composite material was characterized by X-ray diffraction. As shown in Fig. 3**a,** when GO and NaLS are directly mixed, there is a clear GO characteristic peak at about 10° (Guan et al., 2018; Sharma et al., 2017). A diffraction peak is observed at 20°, combined with the peak at 27°, which represents the characteristic peak of NaLS (Zhou et al., 2018; Chen et al., 2016; Xia et al., 2018; He et al., 2015). Compared with the XRD diagram of rGO@NaLS composite material, the GO characteristic peak at about 10° disappear, and multiple continuous peaks appear at about 15°-25° (Fig. 3**a**). It is preliminarily believed that this is caused by the coincidence of the characteristic peaks of rGO with different d values and the above-mentioned NaLS characteristic peaks. The d value of these continuous sharp peaks in the rGO@NaLS composite material is about 4 ∼ 6 Å (According to Bragg's equation, $2d\sin\theta = n\lambda$), which exhibits an increasing trend compared with the d value of ordinary rGO (Chen et al., 2018; Sharma et al., 2017). This observation proves the NaLS is inserted into rGO nanosheets.

Moreover, qualitative analysis of the composite material was conducted by Fourier transform infrared spectroscopy. As shown in Fig. 3**b,** the adsorption peaks of GO present characteristic bands at 3300, 1720 and 1410 cm^{-1}, which are ascribed to the oxygen-containing functional groups on GO, which are caused by the stretching vibrations of hydroxyl, carboxyl and carboxylate groups (Liu et al., 2011). In the infrared spectrum of the rGO@CaLS composite, the peak at 3300 cm^{-1} is reduced, and the peaks at 1720 and 1410 cm^{-1} disappear, which proves that the –OH, –COOH and other oxygen-containing functional groups on GO are significantly reduced, which proves that GO is reduced. At the same time, the absorption peak of -SO_3H appeared in the composite material at 1190 and 1068 cm^{-1} (Tang et al., 2018), which proved the existence of NaLS in the composite material.

3.1.3. Tyndall effect and atomic force microscopy

The rGO@NaLS composite material was tested by AFM (Fig. 4**a**), and a clear rGO flake structure appeared, with a height of 5 ∼ 6 nm (Fig. 4**b**) (Pisarkiewicz et al., 2020; Ma et al., 2016). This observation preliminarily verifies the successful compounding of NaLS with rGO nanosheets during GO reduction. As shown in Fig. 4**c**, the rGO@NaLS solution exhibits uniformity and the Tyndall occurrence is observed (The Tyndall effect diagram of rGO solution is shown in Supporting Information **Figure S2**), which proves the presence of lamellar materials. Compared with the rGO solution in Fig. 2, the lamellar rGO is poorly dispersed in the aqueous solution and in a suspension state. This finding proves that the addition of NaLS largely alleviates the poor dispersion of rGO and thereby facilitates its full mixing with the CaAlg solution, as well as reduce the agglomeration of rGO, thus forming pores with increased uniformity.

3.2. Characterization of a rGO@NaLS/CaAlg dense membrane

To observe the adsorption performance of the rGO@NaLS membrane on ethanol, the degrees of swelling of CaAlg, rGO/CaAlg and rGO@NaLS/CaAlg membranes in the ethanol solution were characterized. Fig. 5 presents, a schematic of pure CaAlg **(a)**, NaLS/CaAlg **(b)**, and rGO@NaLS/CaAlg **(c)** membranes. With the addition of NaLS, the color of the membrane turns dark, and it is yellowish brown; with the addition of rGO@NaLS, the color of the membrane turns dark, and it is black. Three kinds of membranes are used, and the stability of each in the ethanol solution is evaluated.

As shown in Fig. 6, with increases in ethanol concentration, the degree of swelling of the three kinds of membranes

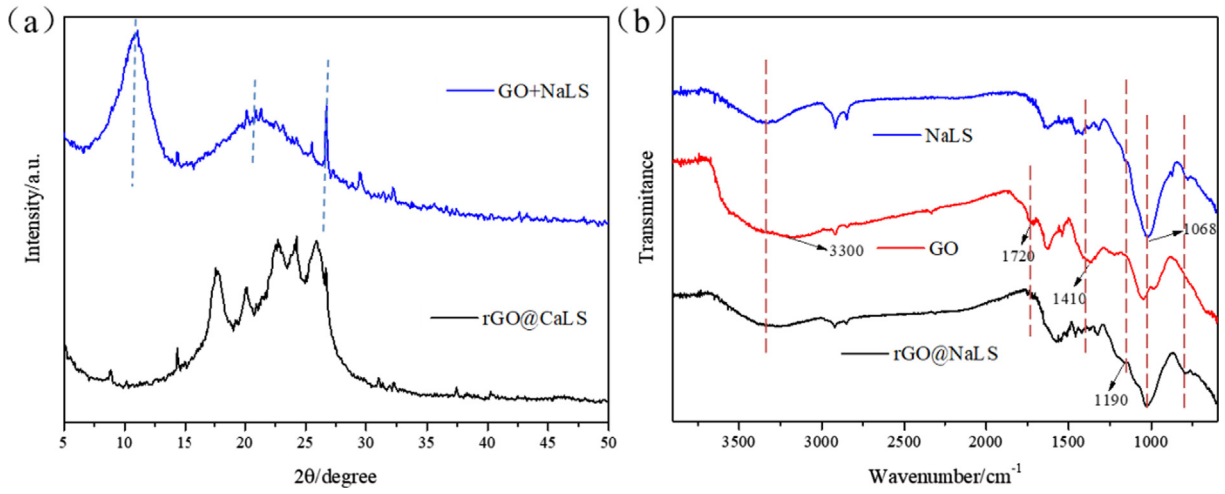

Fig. 3 XRD pattern (a) and FTIR spectra (b) of rGO@NaLS composite material.

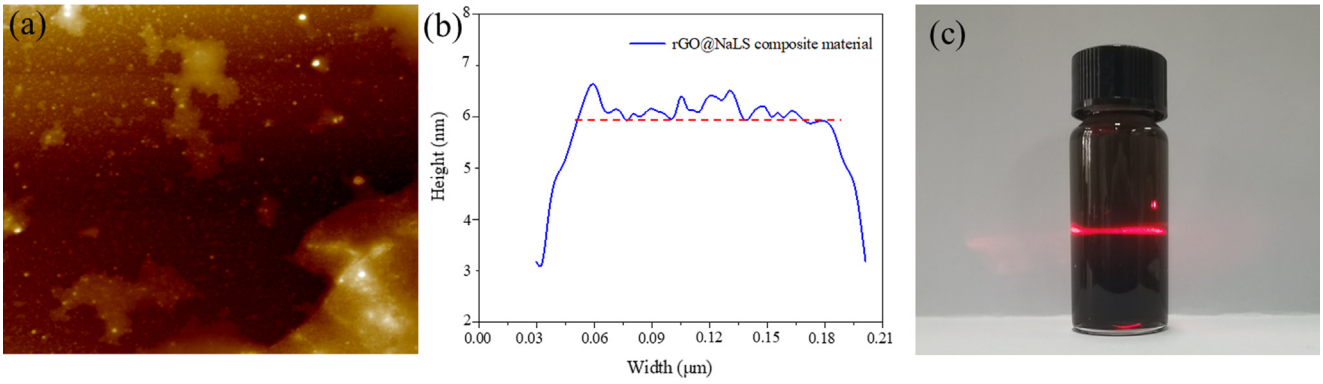

Fig. 4 AFM image (a), thickness distribution (b) and Tyndall effect (c) of the rGO@NaLS composite material.

decreases. In the 90 wt% ethanol, the degree of swelling of the CaAlg membrane is 0.27, whereas that of the rGO@NaLS/CaAlg membrane is 0.17, reflecting a 37% reduction relative to that of the CaAlg membrane. The rGO@NaLS composite material improves the stability of the membrane in the ethanol solution. The membranes, rank by overall degree of swelling are listed as follows: CaAlg > rGO/CaAlg > rGO@NaLS/CaAlg. This sequence indicates that the rGO@NaLS/CaAlg membrane exhibits the highest stability in the ethanol solution and the lowest ethanol adsorption. Both characteristics facilitate ethanol and water separation. The results on the degree of swelling of the CaAlg, rGO/CaAlg and rGO@NaLS/CaAlg membranes in water are shown in **Figure S1** of the Supporting Information. The results indicate that the membranes exhibit higher degrees of swelling in water and quickly reach swelling equilibrium within 2 h. Further, CaAlg, rGO/CaAlg and rGO@NaLS/CaAlg membranes more effectively adsorb water than ethanol.

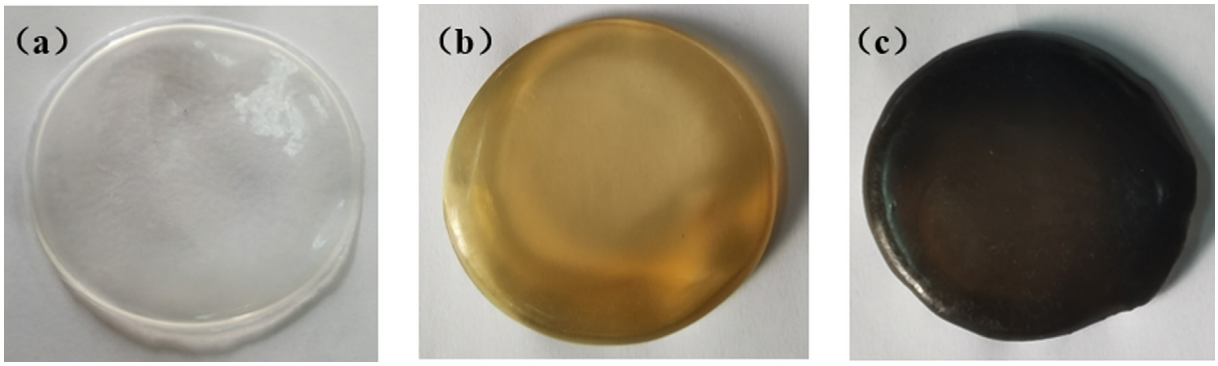

Fig. 5 Schematic of the membranes (a: pure CaAlg membrane; b: NaLS/CaAlg membrane; c: rGO@NaLS/CaAlg membrane.)

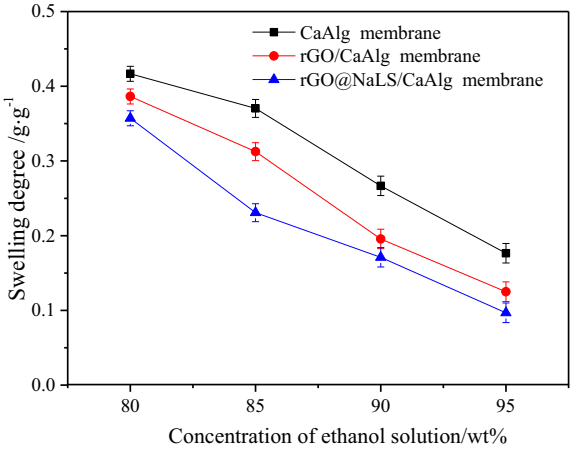

Fig. 6 Degrees of swelling of the CaAlg, rGO/CaAlg and rGO@NaLS/CaAlg membranes at different ethanol concentrations.

3.3. Characterization of the rGO@NaLS/CaAlg composite membrane

3.3.1. Scanning electron microscopy

As shown in Fig. 7, the morphology of the rGO@NaLS/CaAlg membranes with different contents of rGO@NaLS were characterized by scanning electron microscopy. Fig. 7**a** shows a pure CaAlg membrane without rGO@NaLS composite material. When the content of rGO@NaLS is 6 wt% (Fig. 7**b**), only slightly changed on the surface of the membrane. and the graininess is slightly higher than that of the pure CaAlg membrane (Fig. 7**a**). When the rGO@NaLS content was increased to 10 wt% (Fig. 7**c**), a large lamella structure appeared on the surface.

The cross-sectional thickness of membranes after dewatering is around 10 μm. When the content of rGO@NaLS is 6 wt%, the cross-sections of the membrane are arranged tightly, no large gaps are found, and only some denser layered structures are shown (Fig. 7b1); meanwhile, adding 10 wt% rGO@NaLS (Fig. 7**c1**) membrane shows apparent cross-sectional defects in the membrane. The effect of rGO@NaLS on the inside of the membrane was observed by higher resolution SEM (Fig. 7**a2, b2 and c2**). Different rGO@NaLS/CaAlg membranes show apparent internal differences. When the rGO@NaLS content is 6 wt%, the structure is uniform and the layered pores are clearly visible (Fig. 7**b2**); moreover, the excessive rGO@NaLS, internal collapse and structural pores are messy (Li et al., 2021) (Fig. 7**c2**).

3.3.2. Water contact angle

Fig. 8 presents the hydrophilic characterization results of the rGO@NaLS/CaAlg membranes of different rGO@NaLS composite materials. As shown in the figure, when the content

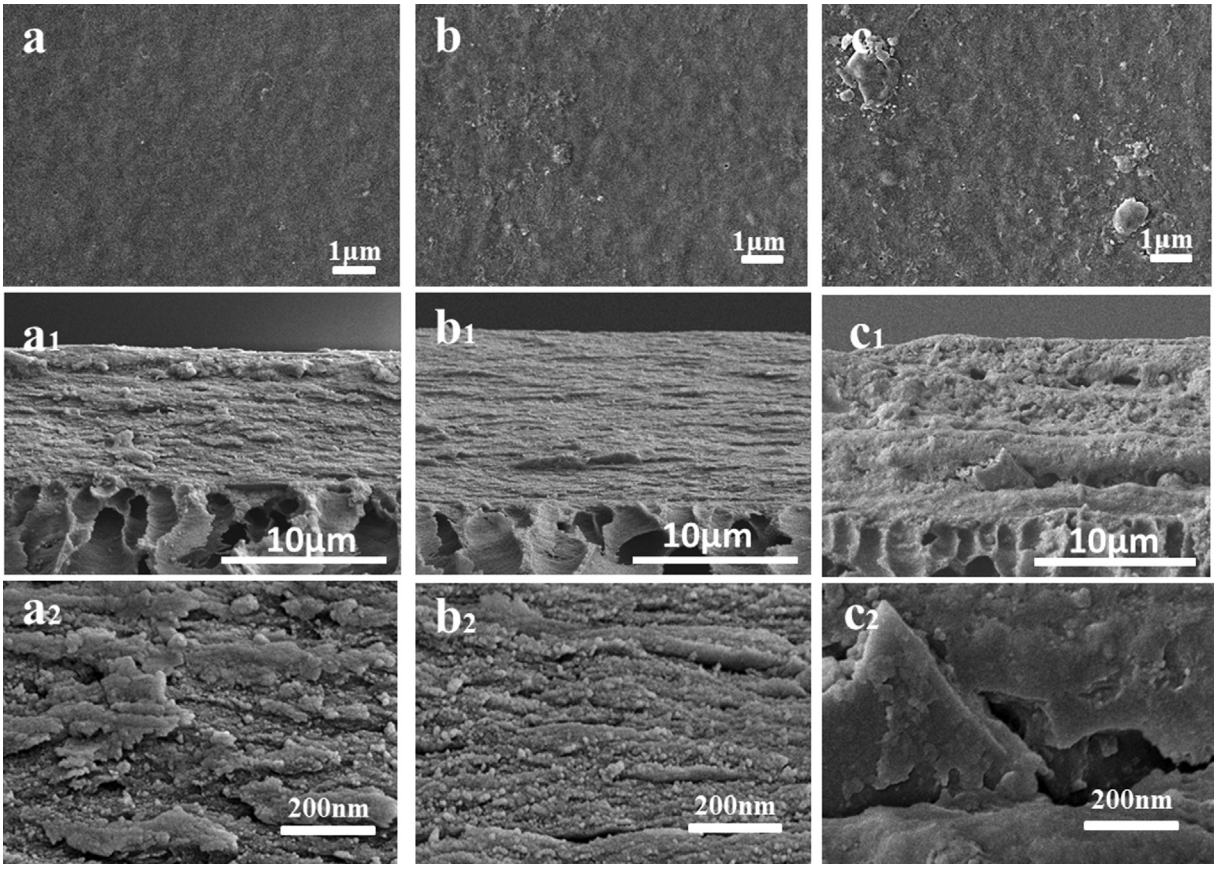

Fig. 7 SEM images of the membrane surfaces and cross-section with the rGO@NaLS/CaAlg membrane. (different rGO@NaLS content: 0% (a, a^1, a^2); 6 wt% (b, b^1, b^2); 10 wt% (c, c^1, c^2)).

of the rGO@NaLS composite material ranges from 0 ~ 8 wt %, the contact angle of the membrane gradually decreases and the hydrophilicity gradually increases. The reason is that NaLS is hydrophilic, and when compounded with the rGO sheet, it increases the hydrophilicity of rGO@NaLS composite material, and adding to the CaAlg matrix can increase the hydrophilicity of the CaAlg membrane. In accordance with the dissolution and diffusion mechanism of the membrane, the hydrophilicity of the rGO@NaLS/CaAlg membrane increases, the ability to dissolve water increases, and the water flux gradually increases; when the content of rGO@NaLS reaches 10%, the contact angle abruptly decreases to 17°, This reduction is due to the excessive content of rGO@NaLS, which led to defects on the surface of the membrane, increased roughness (Fig. 7**c**), and significantly increase hydrophilicity.

3.4. Separation performance of the composite membrane

3.4.1. Effect of rGO@NaLS content

As shown in Fig. 9, the pervaporation performance of the rGO@NaLS/CaAlg membrane was characterized using the dehydration experiment of the ethanol solution. The effect of the content of rGO@NaLS on the selectivity and permeability of the membrane were preliminarily studied. As shown in Fig. 9**a**, when the content of rGO@NaLS ranges from 2 wt % to 6 wt%, the selectivity and permeability of the CaAlg membrane can be simultaneously improved. Moreover, When the content of rGO@NaLS is 6 wt%, the separation factor is 5780, and the permeation flux is 712 $g{\cdot}m^{-2}{\cdot}h^{-1}$. Under the aforementioned condition, the highest selectivity is exhibited (the separation factor and permeation flux of the pure CaAlg membrane 6 and 1.5 times, respectively). Subsequently, the content of rGO@NaLS increases, the selectivity of the rGO@-NaLS/CaAlg membrane decreases, and the permeation flux exhibits an upward trend. When the content of rGO@NaLS reaches 10 wt%, and the permeation flux is 938 $g{\cdot}m^{-2}{\cdot}h^{-1}$.

The changes in ethanol and water fluxes of the rGO@-NaLS/CaAlg membrane are shown in Fig. 9**b**. Moreover, with an increase in the rGO@NaLS content, the water flux

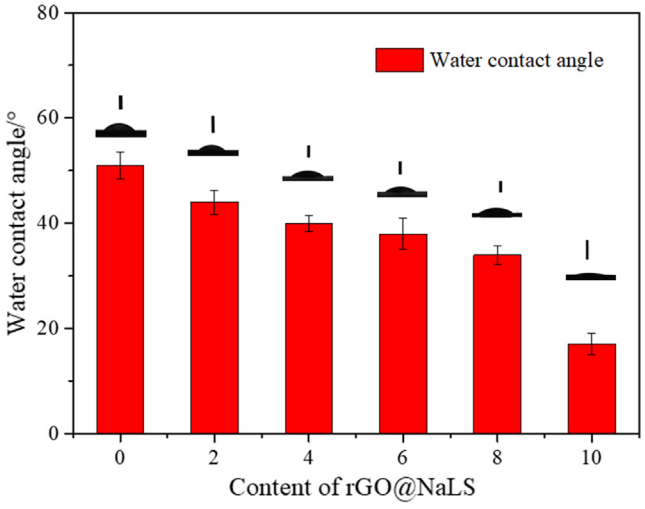

Fig. 8 Water contact angles of the rGO@NaLS/CaAlg membranes with different contents of rGO@NaLS.

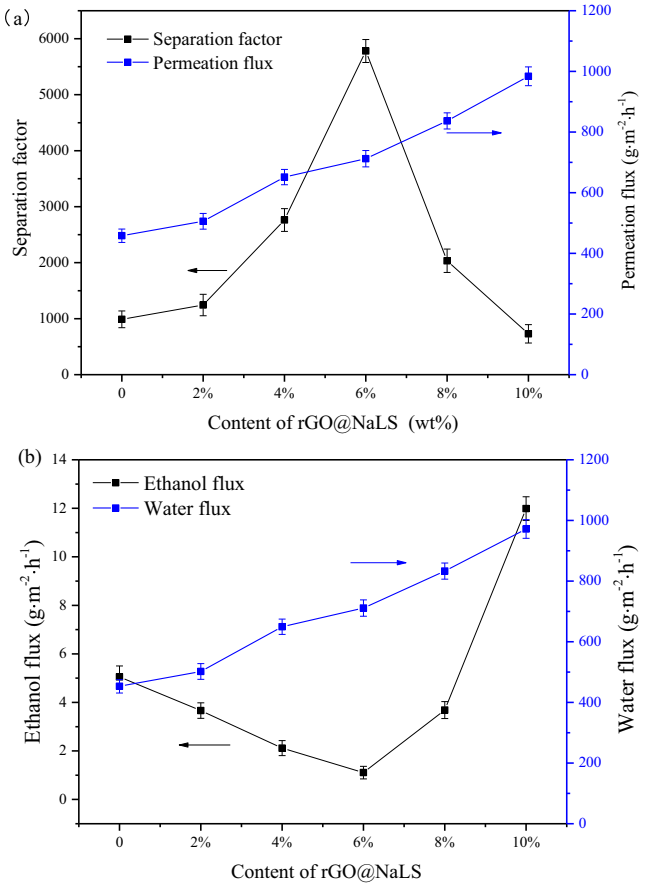

Fig. 9 Pervaporation performance of the rGO@NaLS/CaAlg membranes. (separation factor and permeation flux (a); ethanol and water flux (b)).

increases from 502.1 $g{\cdot}m^{-2}{\cdot}h^{-1}$ to 971.8 $g{\cdot}m^{-2}{\cdot}h^{-1}$, which is consistent with the change trend of the total flux in Fig. 9**a**. The flux of ethanol initially shows a decreasing trend and then increases. When the content of rGO@NaLS is 6 wt%, the flux of ethanol is as low as 1.1 $g{\cdot}m^{-2}{\cdot}h^{-1}$. The best dehydration performance is thus exhibited, and the rGO@NaLS/CaAlg membrane shows the highest selectivity. Subsequently, the excessive content of rGO@NaLS causes membrane defects and increases the ethanol flux.

In accordance with dissolution-diffusion mechanism of the pervaporation membrane, adding rGO@NaLS increases the hydrophilicity of the CaAlg membrane (Fig. 8), and enhances the dissolution/adsorption of water molecules by the membrane. Meanwhile, NaLS combines with rGO sheets to form rGO@NaLS with certain interlayer channels, increasing the diffusion channels of permeating molecules. This allows water molecules to quickly pass through the membrane, and the water flux increases rapidly. The rGO@NaLS/CaAlg membrane is more stable in a high-concentration ethanol solution, and the swelling effect is poor (Fig. 6), and the ethanol molecules are limited by the channel size, when rGO@NaLS is added, the ethanol flux decreases (Fig. 9**b**). The rapid transmission of water molecules also hinders the ethanol molecules to a certain extent. At this time, the total flux and the water flux are consistently increasing. When the rGO@NaLS content exceeds 6 wt%, large gaps appear in the cross-section of the

membrane (Fig. 7**c1**), the molecular transmission channel further expanded, and both the ethanol flux and the water flux increase. When rGO@NaLS content is 6 wt%, the highest separation factor of the membrane was the observed.

3.4.2. Effect of temperature on the rGO@NaLS/CaAlg composite membranes

As shown in Fig. 9, the best pervaporation performance is observed when the rGO@NaLS composite material content is 6 wt%, so this type of membrane is selected for analysis in the following discussion. As shown in Fig. 10, the influence of operating temperature (40 ~ 70) on ethanol dehydration performance is illustrated. As the temperature rises, the selectivity and permeability of the rGO@NaLS/CaAlg membrane increase. As shown in the figure, the separation factor and permeation flux reach 5569 and 802 $g{\cdot}m^{-2}{\cdot}h^{-1}$, respectively, at 70 ℃ (Fig. 10**a**). However, the ethanol and water flux of the rGO@NaLS/CaAlg membrane varies, and the water flux changes from 494.7 $g{\cdot}m^{-2}{\cdot}h^{-1}$ to 798.5 $g{\cdot}m^{-2}{\cdot}h^{-1}$, and the ethanol flux from 3.2 $g{\cdot}m^{-2}{\cdot}h^{-1}$ to 3.5 $g{\cdot}m^{-2}{\cdot}h^{-1}$, but such a change is not significantly. (Fig. 10**b**)

With regard to changes in ethanol and water flux, fitting according to the Arrhenius equation, the activation energy of the water flux is 14.1 kJ/mol, and the activation energy of the ethanol flux is 2.34 kJ/mol (Fig. 11). The positive and negative values of the activation energy are consistent with the flux change, that is, water and ethanol flux increase with the increase in temperature. (The detailed calculation process has been added to the Supporting Information)

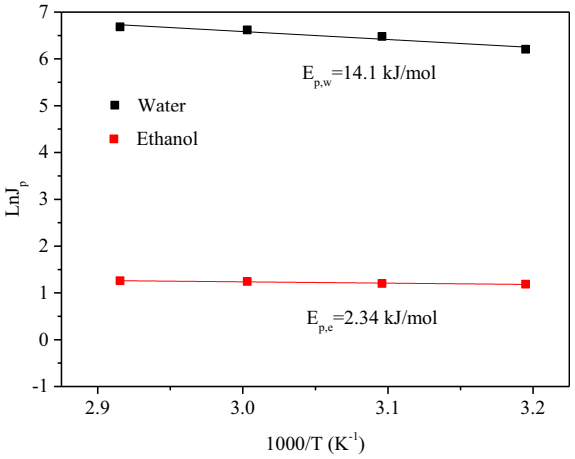

Fig. 11 Arrhenius plots of water and ethanol.

€The reason for this occurrence is that as the temperature rises, high temperature provides a driving force for molecular transport and accelerates the diffusion of molecules inside the membrane. The addition of rGO@NaLS improves the swelling resistance and hydrophilicity of the membrane in the ethanol solution, and the change in water flux is more significant.

3.4.3. Analysis of pervaporation performance

The aforementional experiments confirm that the rGO@NaLS composite material can improve the selectivity and permeability of the CaAlg membrane. This study also considers whether the addition of rGO alone affects the permeability of the CaAlg membranes. As shown in Fig. 12, after the addition of rGO nanosheets, the lamellar structure of the rGO broadens the molecular transport channels, and the selectivity and permeability are improved (the selectivity and permeability are increased by 50% relative to that of pure CaAlg membranes). However, owing the strong affinity between the rGO nanosheets, poor dispersion, and easy stacking in polymer CaAlg, the degree of improvement is low. After adding

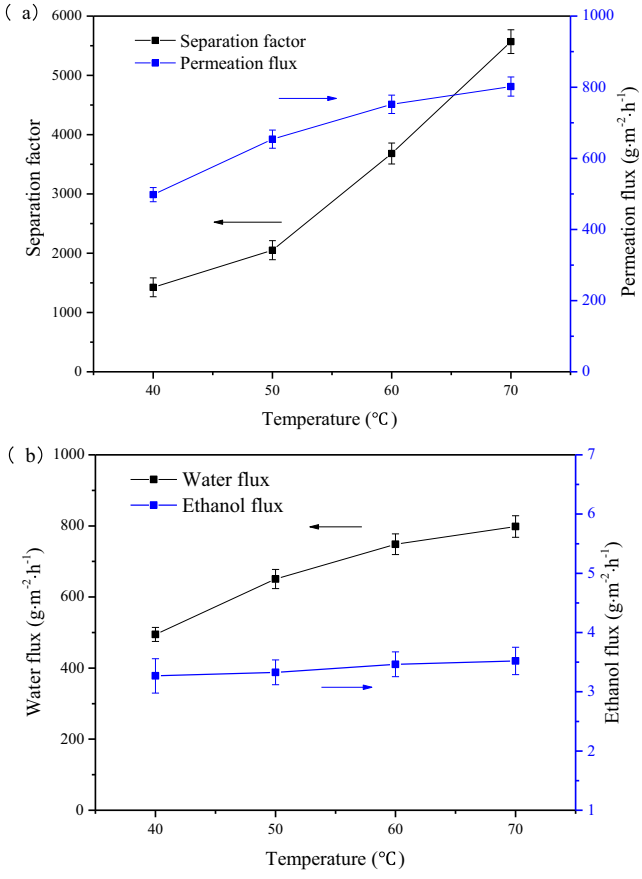

Fig. 10 Dehydration effects of the rGO@NaLS/CaAlg membrane at different operating temperatures.

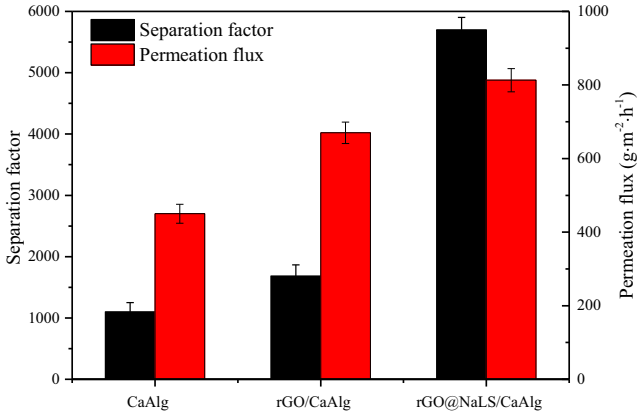

Fig. 12 Comparison of the performance of the pure CaAlg, rGO/CaAlg and rGO@NaLS/CaAlg membranes.

Table 1 Dissolution coefficients, diffusion coefficients and permeability coefficients of water in the membranes.

Membrane	S_{water}	$D_{water} \times 10^{14}/m^2 \cdot s^{-1}$	$P_{water} \times 10^{14}/m^2 \cdot s^{-1}$	R^2
CaAlg	1.298	1.483	1.924	0.9985
rGO/CaAlg	1.186	1.877	2.226	0.9986
rGO@NaLS/CaAlg	1.425	4.034	5.723	0.9990

rGO@NaLS, the selectivity and permeability of the membrane are improved. Compared with pure CaAlg membrane, the selectivity and permeability are increased by 418% and 75%, respectively. The reason is that the LS^{-1} group of NaLS exhibits an affinity for the aromatics of rGO, and can be assembled with the flat layer of rGO to form a composite structure, which improves the dispersion of rGO@NaLS in the CaAlg matrix. According to the principle of dissolution and diffusion, the hydrophilicity of rGO@NaLS can improve the dissolution of water molecules, and the hydrophobic channels between rGO sheets can quickly diffuse water molecules, considerably improving the transmission of water molecules.

3.4.4. Calculation of the dissolution and diffusion coefficients of the membranes

On the basis of the dissolution-diffusion theoretical model, the formula can be expressed as follows:

$$S = \omega_\infty \tag{4}$$

$$D = \frac{\pi}{t}\left(\frac{h\omega_t}{4\omega_\infty}\right)^2 \tag{5}$$

$$\frac{\omega_t}{\omega_\infty} = \frac{4}{h\pi^{1/2}}\sqrt{Dt} \tag{6}$$

$$P = D \times S \tag{7}$$

where ω_t (g/g) is the dissolved amount in t seconds, ω_∞ (g/g) is the equilibrium dissolved amount h (m) is the thickness of the cross-linked membrane, S is the solubility coefficient, D is the diffusion coefficient, and P is the permeability coefficient.

Table 1 lists the solubility coefficient (S_{water}), diffusion coefficient (D_{water}) and permeability coefficient (P_{water}) of the three kinds of membranes in an aqueous solution. The rGO/CaAlg membrane has a S_{water} value of 1.186, which is lower than that of the CaAlg membrane, which may be attributable to the hydrophobicity of rGO nanosheets; the D_{water} of the rGO/CaAlg membrane is 1.877, which is higher than that of the CaAlg membrane that is the addition of rGO nanosheets expands the rapid molecular transport channel. This result shows that the addition of rGO enhances the diffusion of permeating molecules and hinders the dissolution of water molecules, but the permeability coefficient increases, indicating that rGO improves the performance of the CaAlg membrane and positively affects its diffusion. Both the solubility and diffusion coefficients of the rGO@NaLS/CaAlg membrane improve, especially the diffusion coefficient, which is 2.6 times that of the pure CaAlg membrane, and the permeability coefficient is significantly improved. The addition of the rGO@NaLS composite material improves the hydrophilicity of the CaAlg membrane (Fig. 8), and the adsorption/dissolution capacity is considerably enhanced. The rGO@NaLS composite material not only widens the diffusion channel in the CaAlg matrix, but also NaLS combines rGO nanosheets to form interlayer channels, further improving the diffusion of molecules.

The permeation performace of rGO@NaLS/SA membrane was further tested for long time (test conditions: 70℃, 90 wt% ethanol solutions). The rGO@NaLS/SA membrane can still maintain a relatively excellent separation effect after 180 h of experiment, with the separation factor of 5125 and the permeation flux of 791.2 $g \cdot m^{-2} \cdot h^{-1}$. The legend analysis of this part of the experiment is in the Supporting Information **Figure S3**

4. Conclusion

In summary, we prepared rGO@NaLS composite materials using a reduction method, and fabricated rGO@NaLS/CaAlg membranes for pervaporation. The introduction of NaLS into rGO not only improves the dispersion of rGO, but also further broadens the interlayer channels of rGO, so that water molecules are transported quickly in the rGO@NaLS/CaAlg membrane, which significantly improving the permeability and selectivity of the CaAlg membrane. The membrane incorporated with 6 wt% rGO@NaLS shows the best performance, and the ethanol concentration reaches 99.8% (the separation factor is 5780 and the permeation flux is 712 $g \cdot m^{-2} \cdot h^{-1}$). These results indicate that the manufactured rGO@NaLS can effectively improve the dehydration performance of the CaAlg membrane and may benefit from practical applications. Moreover, rGO@NaLS composite materials are expected to be applicable in other membrane separation fields such as nanofiltration and forward osmosis.

CRediT authorship contribution statement

Saisai Li: Conceptualization, Investigation. **Yaru Wu:** Investigation. **Xia Zhan:** Validation, Writing – review & editing. **Jiding Li:** Resources. **Jiandu Lei:** Resources. **Jing He:** Writing – review & editing. **Luying Wang:** Conceptualization, Resources, Supervision, Writing – review & editing.

Declaration of Competing Interest

The authors declare that they have no known competing financial interests or personal relationships that could have appeared to influence the work reported in this paper.

Acknowledgments

This work was supported by the Fundamental Research Funds for the Central Universities (No.2021ZY19), Open Research Fund Program of Key Laboratory of Cleaner Production and Integrated Resource Utilization of China National Light

Industry (No. CP-2020-YB7), National Natural Science Foundation of China (Nos. 21736001, 21776153, 21978024), and Beijing Natural Science Foundation (No. 2202034).

Appendix A. Supplementary data

Supplementary data to this article can be found online at https://doi.org/10.1016/j.arabjc.2021.103549.

References

Cao, Y., Hassan, M., Cheng, Y., Chen, Z., Wang, M., Zhang, X., Haider, Z., Zhao, G., 2019. Multifunctional photo-and magnetoresponsive graphene oxide–Fe3O4 nanocomposite–alginate hydrogel platform for ice recrystallization inhibition. ACS Appl. Mater. Interfaces 11 (13), 12379–12388.

Chen, D., Liang, F., Feng, D., Du, F., Zhao, G., Liu, H., Xian, M., 2016. Sustainable utilization of lignocellulose: Preparation of furan derivatives from carbohydrate biomass by bifunctional lignosulfonate-based catalysts. Catal. Commun. 84, 159–162.

Chen, C., Wang, X., Li, M., Fan, Y., Sun, R., 2018. Humidity sensor based on reduced graphene oxide/lignosulfonate composite thin-film. Sens. Actuators, B 255, 1569–1576.

Chen, Z., Zhao, S., Zhao, H., Zou, Y., Yu, C., Zhong, W., 2021. Nitrogen-doped interpenetrating porous carbon/graphene networks for supercapacitor applications. Chem. Eng. J. 409, 127891.

Ding, L., Wei, Y., Li, L., Zhang, T., Wang, H., Xue, J., Ding, L.-X., Wang, S., Caro, J., Gogotsi, Y., 2018. MXene molecular sieving membranes for highly efficient gas separation. Nat. Commun. 9 (1), 1–7.

Eigler, S., Hirsch, A., 2014. Chemistry with graphene and graphene oxide—challenges for synthetic chemists. Angew. Chem. Int. Ed. 53 (30), 7720–7738.

Fan, X., Liu, Y., Quan, X., 2019. A novel reduced graphene oxide/carbon nanotube hollow fiber membrane with high forward osmosis performance. Desalination 451, 117–124.

Guan, K., Liang, F., Zhu, H., Zhao, J., Jin, W., 2018. Incorporating graphene oxide into alginate polymer with a cationic intermediate to strengthen membrane dehydration performance. ACS Appl. Mater. Interfaces 10 (16), 13903–13913.

Guan, K., Liu, Q., Ji, Y., Zhang, M., Wu, Y., Zhao, J., Liu, G., Jin, W., 2018. Precisely Controlling Nanochannels of Graphene Oxide Membranes through Lignin-Based Cation Decoration for Dehydration of Biofuels. ChemSusChem 11 (14), 2315–2320.

Guo, Z., Ran, S., Fang, Z., 2013. Promoting dispersion of graphene nanoplatelets in polyethylene and chlorinated polyethylene by Friedel-Crafts reaction. Compos. Sci. Technol. 86, 157–163.

Hamzah, N., Johary, F., Rohani, R., Sharifuddin, S.S., Isa, M.H.M., 2020. Development of polyethersulfone (PES)/reduced graphene oxide nanocomposite nanofiltration membrane. PES 1 (21), 70.9.

He, K., Lou, T., Wang, X., Zhao, W., 2015. Preparation of lignosulfonate–acrylamide–chitosan ternary graft copolymer and its flocculation performance. Int. J. Biol. Macromol. 81, 1053–1058.

Kai, D., Zhang, K., Jiang, L., Wong, H.Z., Li, Z., Zhang, Z., Loh, X. J., 2017. Sustainable and antioxidant lignin–polyester copolymers and nanofibers for potential healthcare applications. ACS Sustainable Chem. Eng. 5 (7), 6016–6025.

Kuzminova, A.I., Dmitrenko, M.E., Poloneeva, D.Y., Selyutin, A.A., Mazur, A.S., Emeline, A.V., Mikhailovskii, V.Y., Solovyev, N.D., Ermakov, S.S., Penkova, A.V., 2021. Sustainable composite pervaporation membranes based on sodium alginate modified by metal organic frameworks for dehydration of isopropanol. J. Membr. Sci. 626, 119194.

Li, F.; Wang, X.; Yuan, T.; Sun, R. A lignosulfonate-modified graphene hydrogel with ultrahigh adsorption capacity for Pb(II) removal. *Journal of Materials Chemistry A* **2016**, 10.1039. C6TA03779H.

Li, S., Geng, X., Ma, C., Zhan, X., Li, J., Ma, M., He, J., Wang, L., 2021. Improved performance of three-component structure mixed membrane for pervaporation modified by lignosulfonates@ 2D-MXene. Sep. Purif. Technol. 276, 119294.

Li, S., Geng, X., Ma, C., Zhan, X., Li, J., Ma, M., He, J., Wang, L., 2021. Improved performance of three-component structure mixed membrane for pervaporation modified by lignosulfonates@ 2D-MXene. Sep. Purif. Technol. 119294.

Li, Y., Zhang, H., Ma, C., Yin, H., Gong, L., Duh, Y., Feng, R., 2019. Durable, cost-effective and superhydrophilic chitosan-alginate hydrogel-coated mesh for efficient oil/water separation. Carbohydr. Polym. 226, 115279.

Liu, K., Chen, L., Chen, Y., Wu, J., Zhang, W., Chen, F., Fu, Q., 2011. Preparation of polyester/reduced graphene oxide composites via in situ melt polycondensation and simultaneous thermoreduction of graphene oxide. J. Mater. Chem. 21 (24), 8612–8617.

Liu, H., Sun, Y., Yu, T., Zhang, J., Zhang, X., Zhang, H., Zhao, K., Wei, J., 2019. Plant-mediated biosynthesis of iron nanoparticles-calcium alginate hydrogel membrane and its eminent performance in removal of Cr (VI). Chem. Eng. J. 378, 122120.

Liu, M., Zhang, X., Wu, W., Liu, T., Liu, Y., Guo, B., Zhang, R., 2019. One-step chemical exfoliation of graphite to∼ 100% few-layer graphene with high quality and large size at ambient temperature. Chem. Eng. J. 355, 181–185.

Liu, Z., Zhang, H., Eredia, M., Qiu, H., Baaziz, W., Ersen, O., Ciesielski, A., Bonn, M., Wang, H.I., Samorì, P., 2019. Water-Dispersed High-Quality Graphene: A Green Solution for Efficient Energy Storage Applications. ACS Nano 13 (8), 9431–9441.

Liu, W., Zhou, R., Zhou, D., Ding, G., Soah, J.M., Yue, C.Y., Lu, X., 2015. Lignin-assisted direct exfoliation of graphite to graphene in aqueous media and its application in polymer composites. Carbon 83, 188–197.

Ma, H., He, J., Xiong, D.-B., Wu, J., Li, Q., Dravid, V., Zhao, Y., 2016. Nickel cobalt hydroxide@ reduced graphene oxide hybrid nanolayers for high performance asymmetric supercapacitors with remarkable cycling stability. ACS Appl. Mater. Interfaces 8 (3), 1992–2000.

Ma, L., Zhou, M., He, C., Li, S., Fan, X., Nie, C., Luo, H., Qiu, L., Cheng, C., 2019. Graphene-based advanced nanoplatforms and biocomposites from environmentally friendly and biomimetic approaches. Green Chem. 21 (18), 4887–4918.

Mirabedini, A., Ang, A., Nikzad, M., Fox, B., Lau, K.T., Hameed, N., 2020. Evolving Strategies for Producing Multiscale Graphene-Enhanced Fiber-Reinforced Polymer Composites for Smart Structural Applications. Adv. Sci. 7 (11), 1903501.

Park, S.H., Kim, K., Lim, J.H., Lee, S.J., 2019. Selective lithium and magnesium adsorption by phosphonate metal-organic framework-incorporated alginate hydrogel inspired from lithium adsorption characteristics of brown algae. Sep. Purif. Technol. 212, 611–618.

Pisarkiewicz, T., Maziarz, W., Małolepszy, A., Stobiński, L., Michoń, D., Rydosz, A., 2020. Multilayer Structure of Reduced Graphene Oxide and Copper Oxide as a Gas Sensor. Coatings 10 (11), 1015.

Qiu, L., Zhang, X., Yang, W., Wang, Y., Simon, G.P., Li, D., 2011. Controllable corrugation of chemically converted graphene sheets in water and potential application for nanofiltration. Chem. Commun. 47 (20), 5810–5812.

Safarpour, M., Khataee, A., Vatanpour, V., 2015. Thin film nanocomposite reverse osmosis membrane modified by reduced graphene oxide/TiO2 with improved desalination performance. J. Membr. Sci. 489, 43–54.

Sharma, N., Sharma, V., Jain, Y., Kumari, M., Gupta, R., Sharma, S., Sachdev, K., 2017. In *Synthesis and characterization of graphene oxide (GO) and reduced graphene oxide (rGO) for gas sensing*

application, Macromolecular Symposia, Wiley Online. Library, 1700006.

Shende, P., Pathan, N., 2020. Potential of carbohydrate-conjugated graphene assemblies in biomedical applications. Carbohydr. Polym. 117385.

Sheng, J., Yin, H., Qian, F., Huang, H., Gao, S., Wang, J., 2020. Reduced graphene oxide-based composite membranes for in-situ catalytic oxidation of sulfamethoxazole operated in membrane filtration. Sep. Purif. Technol. 236, 116275.

Tang, Q., Zhou, M., Li, Y., Qiu, X., Yang, D., 2018. Formation of uniform colloidal spheres based on lignosulfonate, a renewable biomass resource recovered from pulping spent liquor. ACS Sustainable Chem. Eng. 6 (1), 1379–1386.

Tong, Z., Liu, X., Zhang, B., 2020. Sulfonated graphene oxide based membranes with enhanced water transport capacity for isopropanol pervaporation dehydration. J. Membr. Sci. 612, 118446.

Xia, M., Jin, C., Kong, X., Jiang, M., Lei, D., Lei, X., 2018. Green removal of pyridine from water via adsolubilization with lignosulfonate intercalated layered double hydroxide. Adsorpt. Sci. Technol. 36 (3–4), 982–998.

Yu, J., Zhang, Y., Chen, J., Cui, L., Jing, W., 2020. Solvothermal-induced assembly of 2D–2D rGO-TiO2 nanocomposite for the construction of nanochannel membrane. J. Membr. Sci. 600, 117870.

Zhang, P., Gong, J.-L., Zeng, G.-M., Song, B., Liu, H.-Y., Huan, S.-Y., Li, J., 2018. Ultrathin reduced graphene oxide/MOF nanofiltration membrane with improved purification performance at low pressure. Chemosphere 204, 378–389.

Zhao, B., Yang, S., Deng, J., Pan, K., 2021. Chiral Graphene Hybrid Materials: Structures, Properties, and Chiral Applications. Adv. Sci. 8 (7), 2003681.

Zhao, K., Zhang, T., Chang, H., Yang, Y., Xiao, P., Zhang, H., Li, C., Tiwary, C.S., Ajayan, P.M., Chen, Y., 2019. Super-elasticity of three-dimensionally cross-linked graphene materials all the way to deep cryogenic temperatures. Sci. Adv. 5 (4), eaav2589.

Zhou, F., Feng, X., Yu, J., Jiang, X., 2018. High performance of 3D porous graphene/lignin/sodium alginate composite for adsorption of Cd (II) and Pb (II). Environ. Sci. Pollut. Res. 25 (16), 15651–15661.